



Particle image velocimetry investigation of the flow-field of a 3D turbulent annular swirling decaying flow induced by means of a tangential inlet

Jeremy Pruvost, J. Legrand, P. Legentilhomme, L. Doubriez

► To cite this version:

Jeremy Pruvost, J. Legrand, P. Legentilhomme, L. Doubriez. Particle image velocimetry investigation of the flow-field of a 3D turbulent annular swirling decaying flow induced by means of a tangential inlet. *Experiments in Fluids*, 2000, 29 (3), pp.291-301. 10.1007/s003480000181 . hal-02533980

HAL Id: hal-02533980

<https://hal.science/hal-02533980>

Submitted on 17 Apr 2020

HAL is a multi-disciplinary open access archive for the deposit and dissemination of scientific research documents, whether they are published or not. The documents may come from teaching and research institutions in France or abroad, or from public or private research centers.

L'archive ouverte pluridisciplinaire **HAL**, est destinée au dépôt et à la diffusion de documents scientifiques de niveau recherche, publiés ou non, émanant des établissements d'enseignement et de recherche français ou étrangers, des laboratoires publics ou privés.

Particle image velocimetry investigation of the flow-field of a 3D turbulent annular swirling decaying flow induced by means of a tangential inlet

J. Pruvost, J. Legrand, P. Legentilhomme, L. Doubiez

Abstract Particle image velocimetry (PIV) has been used in order to measure the three mean components and turbulence intensities of the velocity vector in a swirling decaying flow induced by a tangential inlet in an annulus. This kind of flow motion is found to be very complex, exhibiting three-dimensional and non-axisymmetric characteristics coupled with a free decay of the swirling intensity along the flow path, thereby making it difficult to study. A method allowing the measurement of the three components of the velocity flow-field with a standard PIV system with two-dimensional acquisitions, is presented. The evolution of each velocity component between the inlet and the outlet of the annulus is obtained. Furthermore, the PIV technique is extended to the measurement of turbulent characteristics such as turbulent intensities and dimensionless turbulent energy. The main characteristics of the swirling flow are discussed and the swirl number is estimated as a function of the axial distance from the tangential inlet.

List of symbols

e	thickness of the annular gap
$f(l)$	spatial correlation (m)
K	dimensionless turbulent energy [Eq. (7)]
l	displacement coordinate in the correlation plane (m)
Q	volumetric flow rate in the annular cell (m ³ /h)
r	radial position with respect to the annulus axis (m)
R_i	external radius of the inner cylinder (m)
$Re = 2eU/\nu$	Reynolds number [Eq. (2)]
R_o	internal radius of the outer cylinder (m)
Sn	swirl number [Eq. (1)]
T	time delay between laser pulses (s)
$U = Q/(\pi(R_o^2 - R_i^2))$	average velocity in the annulus (m/s)

V_z

u

v

w

u'

v'

w'

U_m

V_m

W_m

x

z_1

ϕ_e

λ

ν

ζ

Λ_x

$\langle \rangle$

—

out of plane velocity (m/s)

axial velocity according to Reynolds decomposition:

$$u(x, r, \zeta, t)$$

$$= \overline{u(x, r, \zeta, t)} + u'(x, r, \zeta, t)$$

$$= U_m(x, r, \zeta) + u'(x, r, \zeta, t) \text{ (m/s)}$$

radial velocity according to Reynolds decomposition:

$$v(x, r, \zeta, t)$$

$$= \overline{v(x, r, \zeta, t)} + v'(x, r, \zeta, t)$$

$$= V_m(x, r, \zeta) + v'(x, r, \zeta, t) \text{ (m/s)}$$

circumferential velocity according to Reynolds decomposition:

$$w(x, r, \zeta, t)$$

$$= \overline{w(x, r, \zeta, t)} + w'(x, r, \zeta, t)$$

$$= W_m(x, r, \zeta) + w'(x, r, \zeta, t) \text{ (m/s)}$$

velocity fluctuation in axial direction (m/s)

velocity fluctuation in radial direction (m/s)

velocity fluctuation in circumferential direction (m/s)

time-averaged value of radial velocity,

$$U_m(x, r, \zeta) = \overline{u(x, r, \zeta, t)} \text{ (m/s)}$$

time-averaged value of circumferential velocity,

$$V_m(x, r, \zeta) = \overline{v(x, r, \zeta, t)} \text{ (m/s)}$$

time-averaged value of axial velocity,

$$W_m(x, r, \zeta) = \overline{w(x, r, \zeta, t)} \text{ (m/s)}$$

axial position with respect to tangential inlet (m)

laser sheet thickness (m)

diameter of the tangential inlet (m)

emission wavelength of the laser beam (m)

kinematic viscosity of water (m²/s)

circumferential position with respect to the tangential inlet axis (radians)

spatial turbulence length (m)

spatial averaging

time averaging

1

Introduction

Computer progress linked to computational fluid dynamics (CFD), visualization and velocity measurement techniques for flow studies, such as particle image velocimetry

(PIV), are now able to provide the main hydrodynamic characteristics of a given flow configuration with sufficient accuracy (Köhler and Weichert 1998; Shi and Chehroudi 1994; Nejad et al. 1988). A usual two-dimensional PIV technique will be used in the present work in order to obtain the main features of a complex three-dimensional flow: the spatial distribution of the mean values and turbulence intensities of the three components of the velocity vector in a swirling decaying flow.

In the studied configuration, the swirling decaying flow is induced by a tangential inlet in an annulus delimited by two concentric cylinders. Following the classification of Gupta et al. (1984), there are two main types of swirling motion:

(1) continuous swirl flows, whose properties are maintained along the flow path and (2) decaying swirling flows, in which the swirl motion is achieved at the inlet of the device and then decays freely along the flow path.

According to Gupta et al. (1984), three major methods can be used to induce swirling decaying flows in tubes or annular geometries: (1) tangential inlet (Legentilhomme and Legrand 1991; Yukawa and Hashimoto 1982; Escudier et al. 1980), (2) guide vanes (swirl vane pack or swirler) (Burfoot and Rice 1984; Sethumadhavan and Raja Rao 1983; Faler and Leibovich 1977) and (3) direct rotation (rotating pipe) (Khoo et al. 1997; Korjack 1985; Simmers and Coney 1979).

The few investigations devoted to this type of flow concurred on the complex nature of the swirling decaying flow. Due to the decay of the swirl motion along the annulus axis, the flow cannot be considered as established along the test cell. When a single tangential inlet is used, the circumferential velocity component w , added to the main movement of the fluid, gives rise to a swirling motion characterized by a three-dimensional flow with non-axisymmetric behaviour, mainly at the entrance of the cell (Aouabed et al. 1994, 1995; Legrand et al. 1997; Farias Neto et al. 1998).

In most studies dedicated to swirling flows, a dimensionless parameter is commonly used to quantify the swirl intensity, the swirl number Sn , which represents the axial flux of swirl momentum divided by the product of the axial flux of axial momentum and the equivalent tube radius, equal to $2e$ for an annulus; it is given by

$$Sn = \frac{\int_{R_i}^{R_o} uwr^2 dr}{2e \int_{R_i}^{R_o} u^2 r dr} \quad (1)$$

where u is the axial velocity, w the circumferential velocity, r the radial coordinate, R_o the internal radius of the outer cylinder and R_i the outer radius of the inner cylinder.

This number is useful to study the decay of the swirling motion with the axial position from the swirl inducer (Hay and West 1975; Gupta et al. 1984) and can often be correlated by means of an empirical relation involving an exponential decay, as confirmed in some theoretical works (Beniseck et al. 1984; Kito and Kato 1985; Kuroda et al. 1981; Ito et al. 1980). Analytical solutions are only available for simple cases and mainly for symmetric swirling flows (Gupta et al. 1984). Otherwise, both axial and tangential velocity profiles have to be known in order to calculate Sn .

Velocity measurements, using common techniques such as hot wire anemometry, are difficult to employ in such

flows because they are very sensitive to the direction of the fluid motion, unlike the PIV technique. Indeed, it is well-known that swirling motion induces a very disturbed flow-field which is not constant in direction, due to the set-up of large eddies (Aouabed et al. 1994, 1995; Farias Neto et al. 1998), and thus, hot wire measurements are difficult to obtain and are ambiguous.

In the present work, PIV is used in order to measure the three components of the fluid motion (axial u , radial v and circumferential w) for a given flow rate and inlet configuration, which is described in the next section. Because the PIV system only gives a two-dimensional representation of the velocity distribution, the third component of the velocity vector, called the out-of-plane velocity, cannot be resolved simultaneously and, thus, some restrictions arise when measuring a highly three-dimensional flow. Those restrictions are discussed in Sect. 2.3. Recent development in PIV has enabled this technique to resolve simultaneously the three components of a flow-field. For example, an experimental approach consists in using two parallel light sheets, each one coded in depth with different colours, and in recording the displacement of tracer particles between both light sheets with CCD colour cameras (Brücker 1996a, b). This kind of technique is difficult to employ because different cameras need optical access, and an accurate synchronization between light pulses and recording by the cameras is needed. When studying flows with complex geometry, such as in an annulus, this technique cannot be employed, because of a limited optical access. Nevertheless, if some criteria are respected, the data loss due to particles moving perpendicularly to the light sheet is minimized and results can then be obtained with good accuracy.

The main turbulent characteristics of a swirling decaying flow have been investigated, using the PIV technique. A number of studies on turbulent flows have been done using PIV, for example in flames (Mungal et al. 1995), in a mixing jar (Cheng et al. 1997), and in free jets (Cenedese et al. 1994) and confined jets (Khoo et al. 1992). A good accuracy of PIV for turbulence measurements has been obtained in these studies by comparing results obtained with laser doppler anemometry (LDA) and PIV (Cenedese et al. 1994). Parameters affecting the measurement uncertainty have been estimated (Host-Madsen and Nielsen 1998) to optimize the accuracy of turbulence measurements. A means of obtaining the three components is by first measuring two components, and then making a second measurement that includes the third component, as described in Sect. 2. Thereafter, the main characteristics of the swirling flow are determined and compared with other works available in the literature.

2

Experimental equipment and methods

2.1

Hydraulic test rig

The annular test section (Fig. 1) is made of two concentric Plexiglas tubes having a total length of 1.5 m. The internal radius of the outer cylinder, R_o , is 50 mm, the outer radius of the inner tube, R_i , being 20 mm. The diameter of the

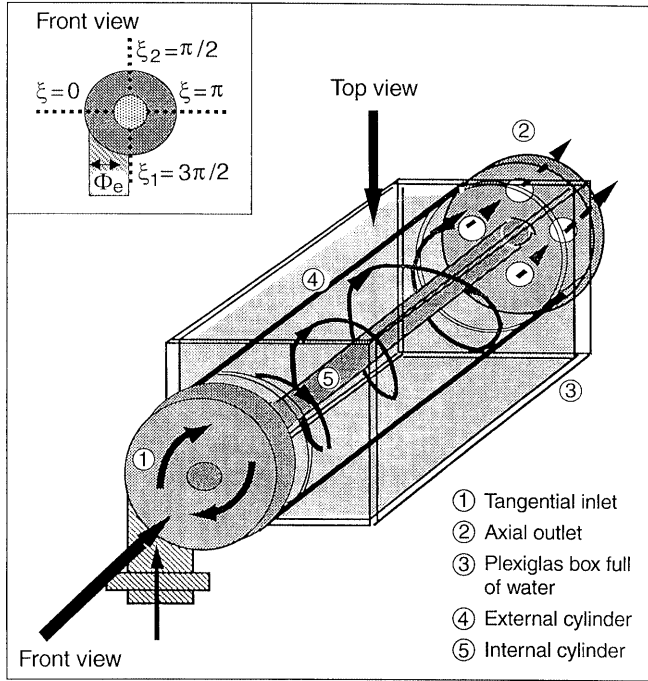


Fig. 1. Test rig with schematic visualization of the swirling flow and circumferential positions investigated

tangential inlet, ϕ_e , is 30 mm, equal to the annular gap width, e , which corresponds to pure swirling flow according to Legentilhomme and Legrand (1991). The outlet of the annulus is of the axial type, so as to not disturb the flow. For all the experimental measurements, the water flow rate is $Q = 2.14 \text{ m}^3/\text{h}$, corresponding to a mean axial velocity in the annulus U of 9 cm/s and a Reynolds number, Re , equal to 5400, where Re is calculated by

$$Re = \frac{2eU}{\nu} \quad (2)$$

In order to simplify the processing of the images, it is useful to minimize optical distortion. Thus, a rectangular Plexiglas box filled with water encloses the annulus. By exposing a flat surface area to the camera, perpendicular to the camera axis, one decreases distortion of the image caused by refraction of light at the curved surface of the outer cylinder (Fig. 1). This technique is commonly used when studying flows in curved geometries separating media with different optical indexes (Saadeh et al. 1997). In this case, it has been verified that image distortion as a result of the refraction could be neglected.

2.2

PIV technique

The system used for PIV is the Dantec device, which allows two-dimensional basic planar measurements. The laser is the Spectra Physics Model 2020 with an emission wavelength of $\lambda = 488 \text{ nm}$ for a maximum emission power of 5 W. The laser beam is shutter-gated to induce laser light pulses, and a thin light sheet is produced by means of an optical lens. The electro-optical shutter is synchronized with a CCD camera Double Image 700, and the camera sensor includes 768×484 light-sensitive pixels. These

images are analyzed with the PIV 2000 Processor to obtain velocity distributions. The statistical method used to obtain velocity distribution is an intercorrelation technique to prevent any flow direction ambiguity.

The tracer used is made of TiO_2 particles with a mean diameter of $30 \mu\text{m}$ and a concentration $C = 0.1 \text{ g/l}$. Because the water relative density of TiO_2 is around 4, such particles are submitted to the effects of the centrifugal force during the swirl motion, which can lead to a displacement of particles towards the outer wall. But circumferential velocities obtained here are low enough to neglect these effects.

When all PIV data are obtained, a post-interrogation procedure is applied to check vectors for erroneous results, because the accuracy of PIV, as for any other measurement technique, is adversely affected by noise. In practice, if experimental parameters are optimized, the number of remaining spurious vectors is low, less than 5%. An analysis of the influence of those vectors on the bias error has concluded that invalid vectors estimate mean velocities towards zero and artificially increase the measured turbulence intensities, because resulting fluctuations are directly added to the mean square (Host-Madsen and Nielsen 1998). The filtering algorithm used is a comparative spatial procedure between each vector of the flow-field with neighboring ones, called the "moving average" by Host-Madsen and McCluskey (1994).

2.3

PIV measurements of mean characteristics

The swirling flow induced by a tangential inlet is highly three-dimensional and non-established with regard to the axial position. Two successive series of measurements are required to obtain the three velocity components. In the first instance, axial and radial velocities are obtained together and, in a second series, axial and tangential velocities are measured. Due to the fact that these three velocities are not achieved simultaneously, this technique can only be applied if the flow is stationary between each series of measurement, which is the case for this swirling flow. The complete procedure can be described as follows: (i) the first series is made in a horizontal axial plane (Fig. 2). Acquisitions simultaneously give axial and radial velocities for the total area seen by the camera. To study the establishment of the swirl motion, axial positions near the inlet, for $x < 900 \text{ mm}$, are investigated. An area close to the outlet is also chosen ($1100 \text{ mm} < x < 1200 \text{ mm}$) to emphasize the global decay of the swirl pattern along the annulus. In Fig. 2, the eight investigated axial positions are shown. Each is 10 cm long and 3 cm wide so as to give a velocity distribution in the entire annular gap width. (ii) The tangential velocity component is not measured in the same way because the camera has to be orthogonal to the investigated velocity component. The position of the laser sheet is shown in Fig. 2. The velocity is tangential to the laser sheet at the center of the acquisition area. Unlike the first series where values are obtained at the same time for different radial positions, the circumferential velocity is achieved for only one radial position, corresponding to the intersection of the laser sheet with the vertical plane passing through the camera axis. By moving the laser sheet

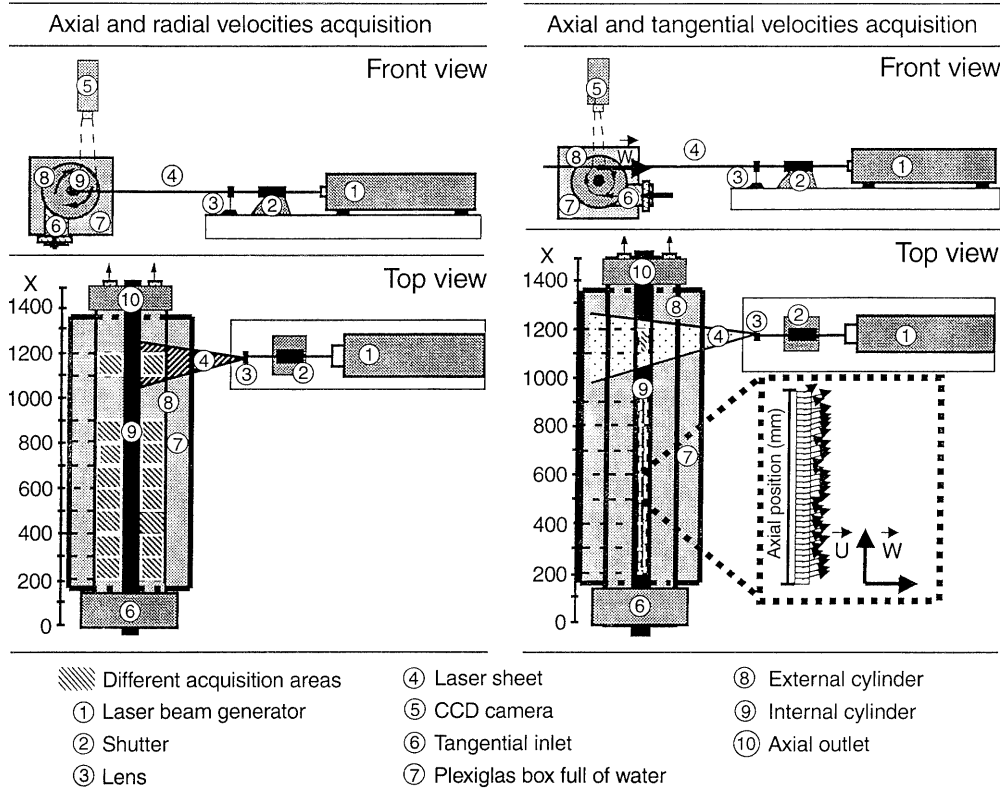


Fig. 2. PIV set-up for both series of measurements

vertically, several radial positions are investigated. Measurements are done for the same axial positions as for axial and radial velocity acquisitions.

For each measurement, two circumferential positions are investigated in order to emphasize the non-axisymmetric behaviour of the flow pattern. The first is located at $\xi_1 = \pi/2$ and the second at $\xi_2 = 3\pi/2$ (see Fig. 1). In order to obtain an accurate value of the mean velocity, 400 acquisitions each $135 \mu s$ for each position previously mentioned are realized and then time averaged. Several previous trials have been done to verify the validity of mean velocity measurements using this number of acquisitions.

The main acquisition parameters, such as the time delay between pulses and the duration of each pulse, are adjusted in order to satisfy classical criteria to obtain accurate results. But if PIV is employed in three-dimensional flows, some additional criteria must be verified. PIV extracts two velocity components of the flow-field by measuring in a laser light sheet the displacement of tracer particles between two successive images acquisitions. So, a first problem is imposed by the particles' motion perpendicular to this laser sheet, resulting in bad correlation when some particles enter or leave the measurement plane between two successive image acquisitions. A second problem is encountered if tracer particles move through the laser sheet but remain in it, because they are not similarly reproduced on two successive images due to the depth of focus, and thus, this leads to an additional error during correlation of the particles' displacement (Raffel et al. 1995). Not taking account of the out-of-plane motion can lead to erroneous results when studying three-dimensional flows. The time between pulses and, thus, the time between successive images, must be small enough to

sample the same particles on both images. This depends on two parameters: the thickness of the laser light sheet and the out-of-plane velocity. It is generally assumed that if the displacement between two successive images remains smaller than the quarter of the laser sheet thickness, the number of particles is sufficient to achieve good correlation. This criterion is expressed by

$$\frac{V_z T}{z_1} < \frac{1}{4} \quad (3)$$

where V_z is the out-of-plane motion, T the time delay between two successive pulses, and z_1 the thickness of the laser light sheet, around $z_1 = 2.5 \text{ mm}$.

Because laser pulses and camera acquisitions are frequency limited, if the out-of-plane motion is too high, PIV cannot be employed under suitable conditions with the usual systems. Here, when measuring both axial and radial velocities, the circumferential velocity due to swirl motion is the out-of-plane velocity and thus, the time between pulses is directly linked to this velocity. For example, a tangential velocity of 30 cm/s leads to a time delay between pulses smaller than $2100 \mu s$, which can be reached with our PIV system. For the study of axial and circumferential velocities as done in the second series of measurements, out-of-plane motion is due to radial velocity, but the latter, being weak, can be neglected.

2.4

PIV measurement of turbulent characteristics

The main turbulent characteristics of a flow-field can be obtained using the PIV technique. Some recent studies have investigated the accuracy of turbulence measurements with such a technique (Host-Madsen and Nielsen

1998). According to these authors, the size of the interrogation area will affect the resolution of the data and, specifically, the determination of velocity fluctuations. For example, large interrogation areas would not allow the study of eddy characteristics at high frequencies. The size of this area will be the critical limit for eddy scale measurements, as for other techniques such as hot wire anemometry, which depends on the wire length, and LDA, for which the results are closely linked to the size of the measurement volume. The smallest interrogation areas are suggested because spatial averaging acts as a low-pass filter, biasing turbulence intensity values. But if the size of these areas decreases, a need for a higher concentration of tracer particles appears to keep a sufficient number of them for good correlation in each interrogation zone. By increasing the seeding density, the influence of the seeding on the flow itself also increases, resulting in two-phase effects and in a reduction of the optical transparency of the flow. Thus, particle concentration and interrogation size area have to be optimized to achieve accurate values of velocity fluctuations. In the Host-Madsen and Nielsen (1998) studies, accuracy in turbulence measurements with PIV is linked to flow conditions. The size of each subdivided interrogation area can be calculated by measuring the integral length scale of turbulence, which is dependent on the eddy dimensions. According to Host-Madsen and Nielsen (1998), for a subdivided interrogation area which is one fifth of the integral length scale, the measured turbulence intensities can be obtained with a relative accuracy of 10%.

Using instantaneous flow fields obtained by PIV, spatial turbulence length scales can be simply obtained. First, the longitudinal correlation has to be calculated as follows (Hinze 1959):

$$f_x(l) = \frac{\langle u'(l_0)u'(l_0 + l) \rangle}{T_x} \quad (4)$$

and then the longitudinal length scale is integrated:

$$\lambda_x = \int_0^x f_x(l) dl \quad (5)$$

where u' is the fluctuation of the axial velocity component, l the displacement coordinate in the correlation plane, T_x the turbulence intensity of the axial velocity, and $\langle \rangle$ represents spatial averaging.

An example of a longitudinal correlation is given in Fig. 3 as calculated on a single instantaneous PIV flow-field by spatial averaging. This result is obtained for only one location in the annulus to evaluate the size of the interrogation area because our purpose is not to fully characterize the turbulent field. The corresponding longitudinal length scale is $\lambda_x = 6$ mm. To verify this result, the procedure was repeated on 25 different acquisitions, and same orders of magnitude were achieved. The resulting subdivided interrogation area was set to 0.87 mm in the axial direction and 1.05 mm in the radial direction, corresponding to a 64×64 pixels² subdivided interrogation area for a total dimension of the acquisition area of 10.8 mm in the radial direction and 6.3 mm in the axial direction with no overlapping.

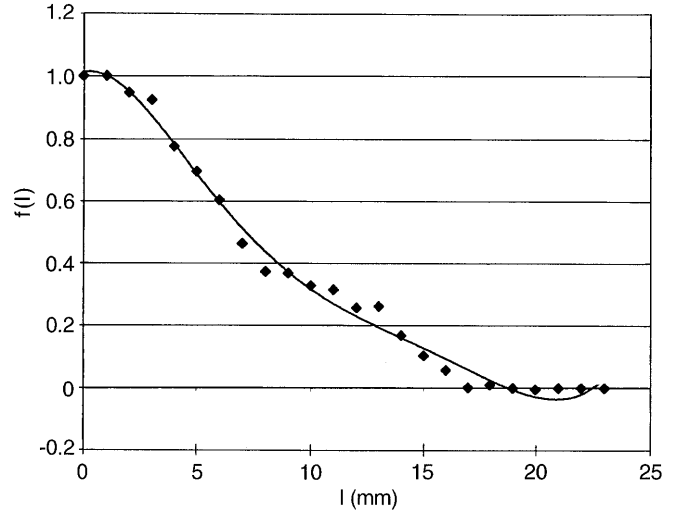


Fig. 3. Spatial longitudinal correlation of axial velocity fluctuations $f(l)$ for $543 < x < 573$ mm, $r = 35$ mm, $\zeta = 3\pi/2$

To establish the validity of this technique for an accurate measurement of turbulent intensities, an additional series was made with no swirl motion, using a radial inlet instead of a tangential one. Thus, the flow generated is mainly an axial annular flow. Turbulence intensities were calculated for only a single axial position, far from the inlet at $x = 1043$ mm, where inlet effects are less sensitive. For turbulent flows in pipes, usual values of turbulence intensities are around 10% and less (Hinze 1959). Results depicted in Fig. 10 using a radial inlet are in good agreement with this value, assuming that the radial inlet still induces small hydrodynamic perturbations in the flow. This validates the procedure employed to obtain turbulence characteristics in swirl flow.

To obtain the radial evolution of turbulent characteristics for the largest part of the gap width, three different series of acquisitions are required: one for $r = 21.5$ – 31.5 mm, the second for $r = 30$ – 40 mm and the last one for $r = 38.5$ – 48.5 mm. In order to analyze the turbulence decay along the axis, three axial positions are investigated: the first portion near the inlet at $x = 93$ mm, the second portion at $x = 543$ mm and the last portion close to the outlet at $x = 1043$ mm. Using the same procedure described to obtain the mean velocities, turbulence intensities are achieved with an ensemble averaging procedure of 2000 filtered acquisitions for each investigated position to reduce the uncertainty of the statistical treatment. Turbulence intensities T_x , T_y and T_z are calculated by (Hinze 1959)

$$T_x = \frac{\sqrt{\overline{u'^2}}}{U}, \quad T_y = \frac{\sqrt{\overline{v'^2}}}{U} \quad \text{and} \quad T_z = \frac{\sqrt{\overline{w'^2}}}{U} \quad (6)$$

where u' is the instantaneous fluctuation of the axial velocity component, v' the radial one and w' the circumferential, U being the average velocity in the annulus, and $(\overline{\quad})$ denotes a time averaging.

To emphasize the overall decay of the turbulence, the dimensionless turbulent energy is calculated by (Clayton and Morsi 1985)

$$K = (T_x^2 + T_y^2 + T_z^2) \quad (7)$$

3 Results and discussion

Figure 4 compares the axial velocity component obtained with both series of measurements defined in Sect. 2.3. Nearly the same values are achieved using any of the data series. It validates the use of such procedures to measure the three mean velocities with a two-dimensional PIV method.

The evolutions of the three mean velocity components are shown in Figs. 5 and 6 for the circumferential positions $\xi_1 = 3\pi/2$ and $\xi_2 = \pi/2$, respectively. The complex behaviour of the swirl motion is emphasized, especially near the tangential inlet at the axial position $x = 500$ mm. The main movement is set by the circumferential velocity, giving rise to the swirling motion around the inner cylinder. This velocity component decreases with axial position but always remains greater than the axial component in our test facility. A radial mean velocity appears, due to large eddies induced by the tangential inlet, which rapidly decreases to zero, emphasizing the dependence of the swirling motion with the axial position. According to studies on swirling flows (Gupta et al. 1984; Farias Neto 1997; Farias Neto et al. 1998), the radial velocity is the weakest component.

Close to the tangential inlet, for $x < 800$ mm, the maxima of both tangential and axial velocities are located near the outer wall, and an increase in axial position results in shifting the maxima towards the center of the annular gap. This can be explained by the effects of the centrifugal force, induced by the tangential inlet. They are greater near the swirl inducer, where the incident swirling motion is more sensitive near the outer wall. Another important characteristic already seen by Aouabed et al. (1994, 1995) in visualization studies using a dot paint

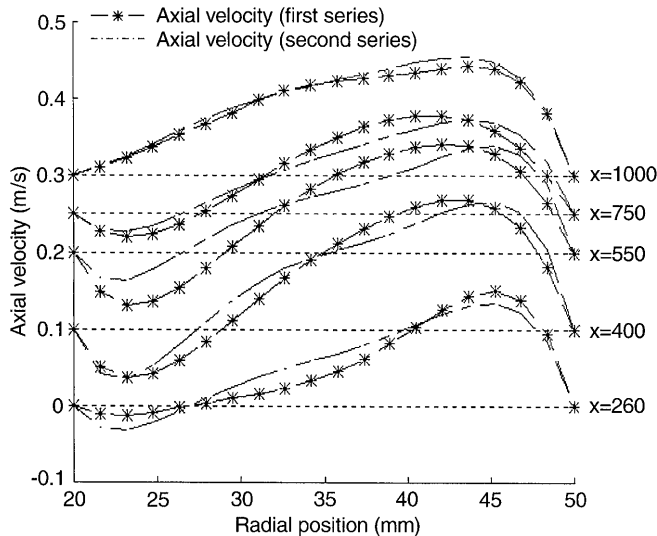


Fig. 4. Axial velocity obtained with the two methods of measurements: first series corresponding to axial and radial velocity acquisitions and second series used for circumferential and axial velocity acquisitions

method appears: a flow reversal (negative axial velocity) is observed near the inner wall, and then vanishes far from the inlet where the effects of the centrifugal force become less important. A very high maximum of axial velocity results in a great recirculating zone, as shown in Fig. 7, where velocity profiles are shown for several axial positions and for the two azimuthal locations, $\xi_1 = \pi/2$ and $\xi_2 = 3\pi/2$.

If the swirl number S_n is considered, the same conclusions can be drawn. Figure 8 shows the evolution of S_n for the two circumferential positions in the annulus as a

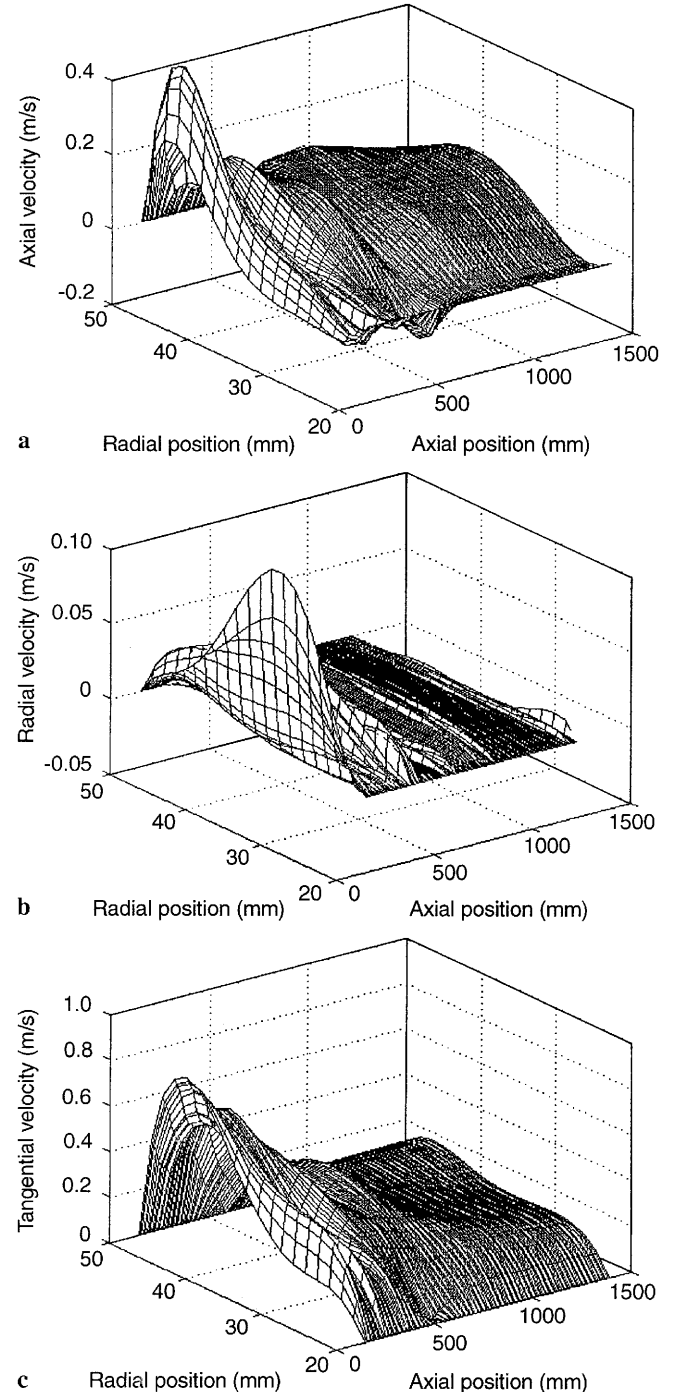


Fig. 5a-c. Spatial distribution of mean velocities for $\xi = 3\pi/2$: a axial velocity, b radial velocity, c circumferential velocity

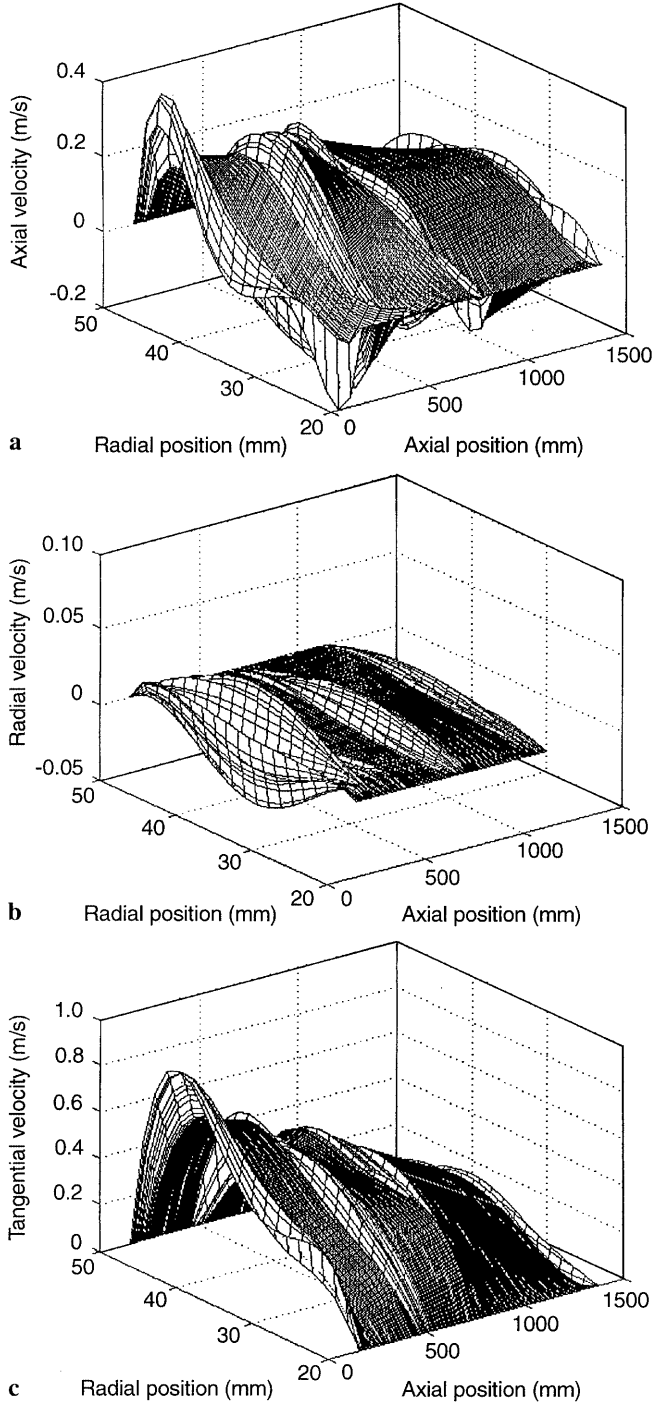


Fig. 6a-c. Spatial distribution of mean velocities for $\xi = \pi/2$: a axial velocity, b radial velocity, c circumferential velocity

function of the axial position from the tangential inlet. Because there is no axisymmetry, evolutions are different for both values of ξ , and near the inlet the important flow disturbance results in large Sn variations, depending on the angular position with respect to the tangential inlet axis. Sn is thus a useful parameter to characterize swirling decaying flows. These results qualitatively agree with previous works (Farias Neto 1997; Farias Neto et al. 1998; Aouabed et al. 1994, 1995). When the flow is not axisymmetric, it is necessary to integrate Eq. (1) along all cir-

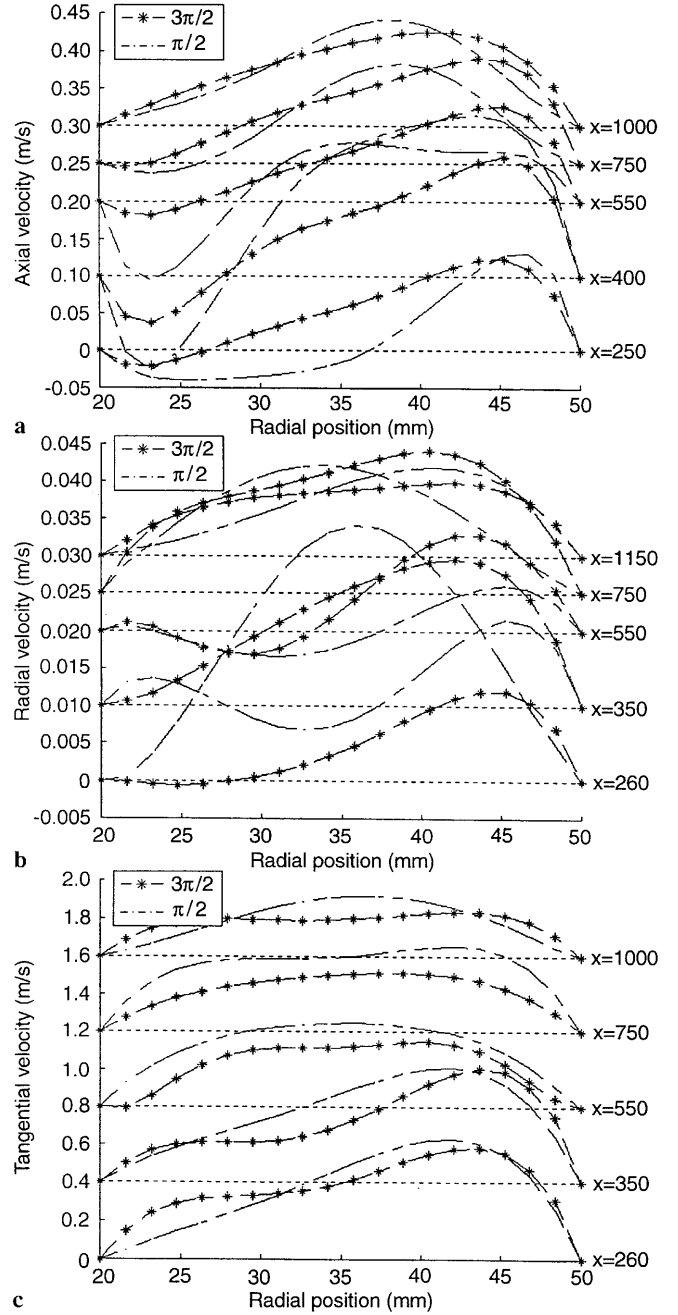


Fig. 7a-c. Mean velocity profiles for different axial positions and both circumferential positions. a Axial velocity, b radial velocity, c circumferential velocity

cumferential positions in order to obtain an average value of Sn . Because only two circumferential positions are investigated, the mean value of Sn shown in Fig. 9 can only be considered as an approximate value. According to several studies on the decay of swirling motions (Gupta et al. 1984), after an integration over all circumferential positions, the Sn evolution can be correlated by means of an exponential decay

$$Sn = a \exp(-bx/2e) \quad (8)$$

However, as shown in Fig. 8, near the inlet, the Sn evolution obtained here cannot be perfectly fitted using this

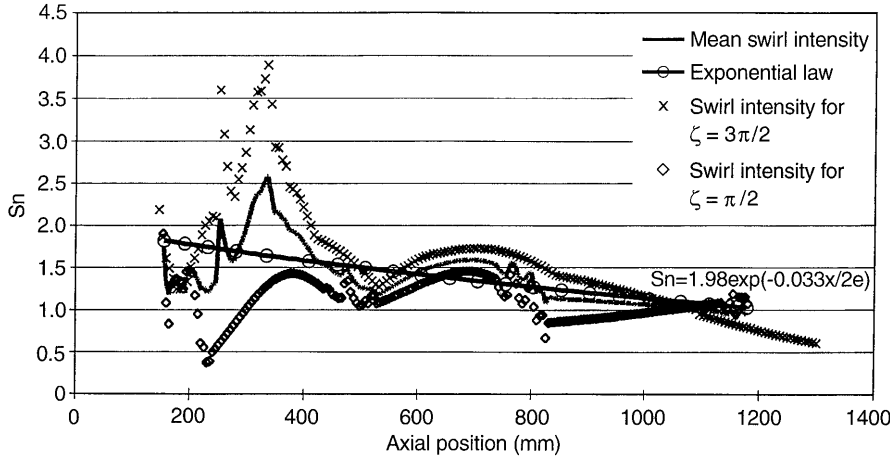


Fig. 8. Evolution of the swirl number

kind of equation. This is easily explained because only two circumferential positions are investigated, and the flow pattern is highly non-axisymmetric near the inlet, where the flow is strongly perturbed by the tangential jet flow (Aouabed et al. 1994, 1995; Legrand et al. 1997). Only approximate parameters a and b can thus be obtained, using a least square method:

$$Sn = 1.98 \exp(-0.033x/2e) \quad (9)$$

With a higher number of angular positions, the accuracy of these results will be improved. Some numerical values were obtained by Farias Neto et al. (1998) for a swirling flow induced by a tangential inlet in an annulus. Their results are available only for laminar conditions, from $Re = 200$ to $Re = 650$, and with different geometrical characteristics: a gap width $e = 7$ mm, $e/R_i = 0.38$ and an inlet diameter $\phi_e = 12.5$ mm. For $Re = 200$, these authors obtain $a = 1.63$ and $b = 0.21$, and for $Re = 650$, $a = 1.55$ and $b = 0.14$. Aouabed et al. (1994) estimated the Sn evolution using a dot paint method for the determination of the streamline angle. In their studies, they found, for $Re = 1194$, a parameter $b = 0.07$, and for $Re = 1994$, $b = 0.049$. Both parameters are sensitive to the geometry and to the hydrodynamic conditions, especially a , which is linked to the initial swirl intensity. Thus, only a rough comparison can be made. Parameter b shows the decay of the swirl motion along the annulus. According to these studies, if Re increases, b decreases because higher initial circumferential velocities in the annulus lead to a greater swirl motion persisting higher up in the annulus. This is in agreement with results obtained here, because with a higher Reynolds number, b is smaller than the values obtained in the previously mentioned studies.

Figure 9 shows that a tangential inlet induces a swirling flow that enhances turbulent intensities in the annulus for the same flow rate. This is in agreement with other works dedicated to swirl motion using different geometric conditions or inlet blowing (Clayton and Morsi 1984, 1985; Nejad et al. 1988; Algifri et al. 1988), and with wall turbulence measurements obtained by Aouabed et al. (1995). Turbulence intensity can be enhanced by a factor greater than 5, especially near the inlet. All along the length of the annulus, turbulence intensities always remain significant

for the three velocity components, compared with those obtained using a radial inlet.

Variations of turbulence intensities along the radial coordinate are small. It has to be specified that the turbulence intensities cannot be accurately determined in wall regions by the technique employed here due to wall adhering effects of particles. In this case, the assumption that particles perfectly follow the flow is biased. Therefore, other techniques have to be used, as reported by Legrand et al. (1997), who employed an electrochemical method to investigate wall turbulence. In confined flows, it is known that turbulence intensities are greater in the wall region than in the core of the flow (Hinze 1959). For example, in pipes, these wall intensities can reach values three times higher than in the centre core. Wall turbulence values obtained by Legrand et al. (1997), around 50–80%, are greater than those obtained in the present study in the core region, which vary between 20 and 50%. Thus, the results of both studies are complementary.

In comparing results for each velocity fluctuation component in Fig. 10, it can be noted that close to the inlet the turbulence intensity of the circumferential velocity is always greater than that of the axial component, the radial velocity component being the weakest. Due to the decay of the swirl motion, the circumferential turbulence intensity decreases rapidly to values close to those of the axial and radial velocity components. Far from the inlet, the turbulence behaviour appears almost isotropic. The anisotropic feature of the turbulence is emphasized near the inlet, where considerable swirling motion dominates (Fig. 10).

Finally, Fig. 11 shows the overall decay of dimensionless turbulence energy. As for the swirl intensity, this decay can be fitted using an exponential law. The overall decay of dimensionless turbulent energy K [Eq. (7)] follows:

$$K = 0.58 \exp(-0.109x/2e) \quad (10)$$

To compare both evolutions of the swirling number and of the dimensionless turbulence energy, they are divided by their maximum value, i.e. the pre-exponential coefficient in the fitting equations, presented in Fig. 11. It can be seen that the dimensionless turbulence energy decays more rapidly than the swirling number. If the dimensionless turbulent energy, calculated with turbulence intensities

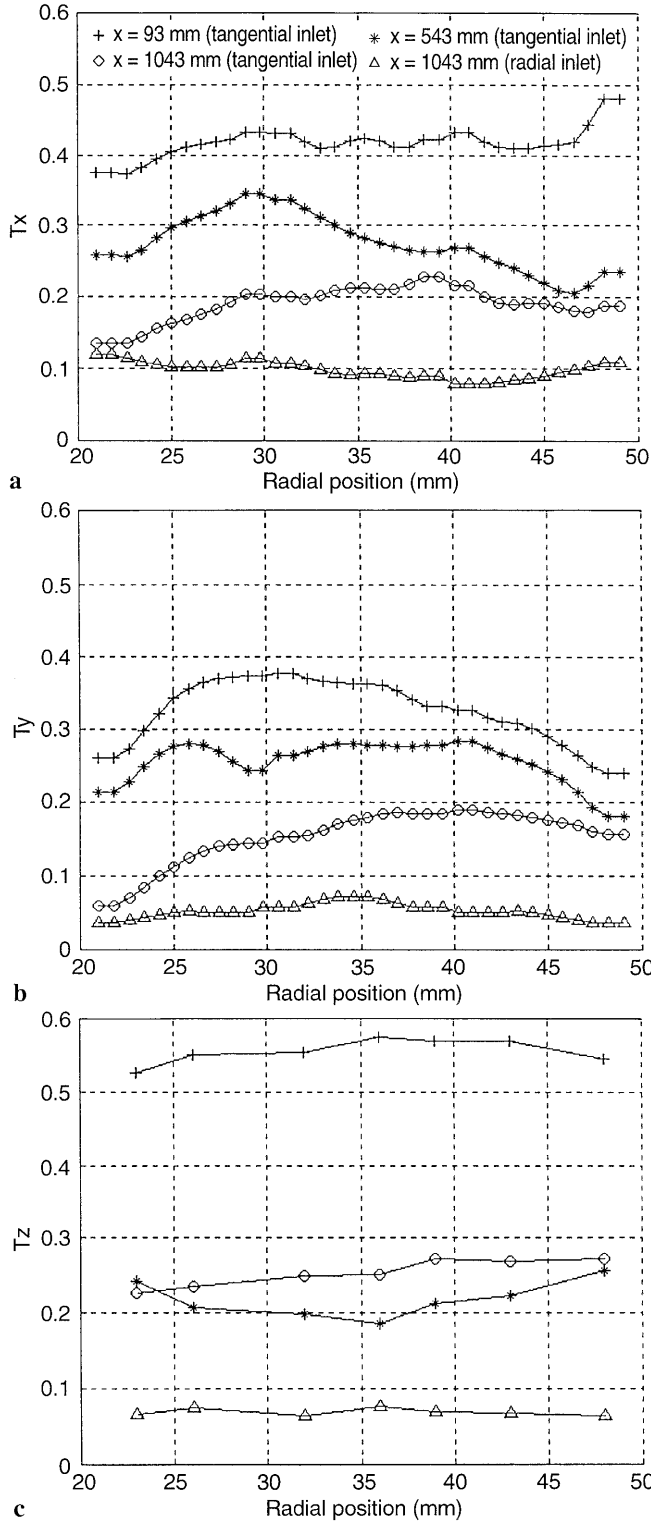


Fig. 9a–c. Turbulence intensities for each velocity component. a Axial velocity, b radial velocity, c circumferential velocity

obtained with the radial inlet, is considered (results of Fig. 9), it can be assumed that this value will be the limit of the dimensionless turbulent energy decay (Fig. 11). Although the swirling motion remains all along the annulus axis, effects on turbulence decrease rapidly. Thus, relation (9) can only be used from an axial distance where the swirl intensity cannot be neglected. When a sufficient

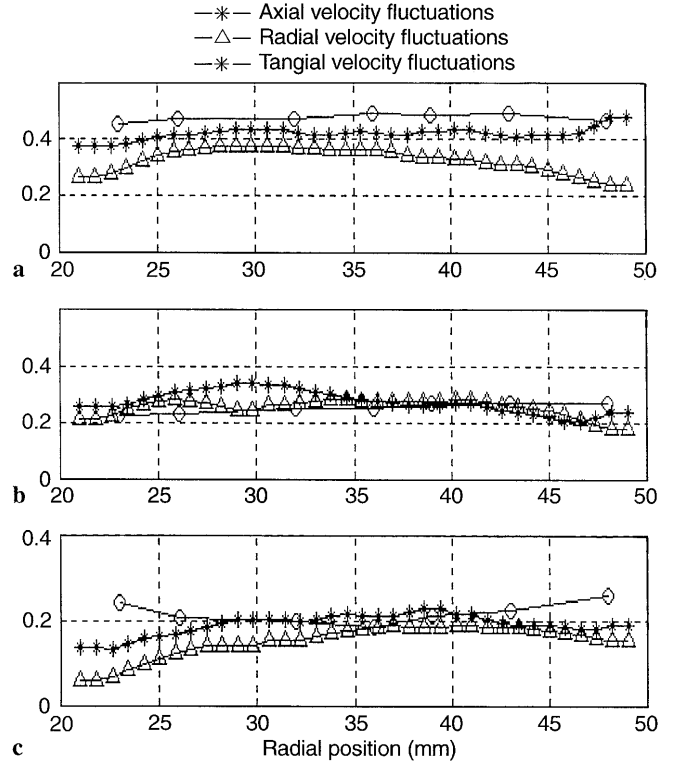


Fig. 10a–c. Axial evolution of turbulence intensities: a $x = 93$ mm, b $x = 543$ mm, c $x = 1043$ mm

length is reached, corresponding to the vanishing of the swirling motion, we can assume that a constant value of the dimensionless turbulence energy will be obtained. This constant value will be the same as for a fully developed turbulent axial flow in an annulus, under the same hydrodynamic conditions, thus corresponding to turbulence intensities less than 10%. Using relation (9) to approximate the axial distance necessary to reach the dimensionless turbulent energy obtained in an axial turbulent flow (i.e. the value obtained with the radial inlet) gives a length of around 1560 mm. Thus for the total length of 1.5 m of the annulus, it is interesting to notice that the effects of the swirl motion on turbulence cannot be neglected.

4 Conclusion

In this study, a complex flow with a three-dimensional behaviour is investigated using PIV measurements. The three mean velocities are easily obtained for different positions where other methods, such as hot wire anemometry, are difficult to use in this kind of geometrical configuration. With the flow being stationary and using two different methods of measurement, the three velocity components can be obtained, although PIV is a two-dimensional method of acquisition. In addition, by satisfying some criteria on the size of the subdivided acquisition area, turbulent characteristics such as turbulent intensities and dimensionless turbulent energy are obtained. The evolution of the characteristics of each component agrees with previous works dedicated to swirling motions, and the main characteristics of swirling decaying flow are observed.

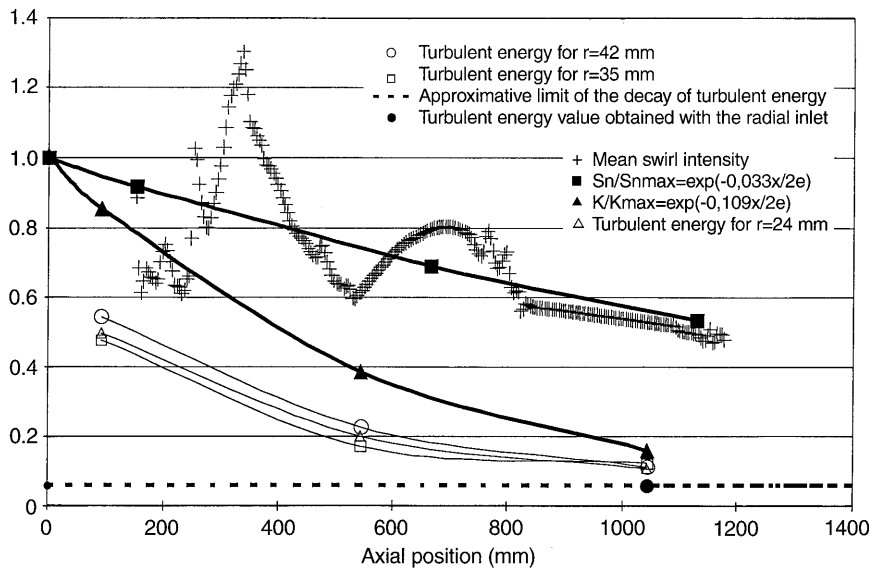


Fig. 11. Axial evolution of dimensionless turbulent energy for three radial positions and of $S_n/S_{n_{\max}}$ and K/K_{\max} with $S_{n_{\max}} = 1.98$ and $K_{\max} = 0.58$

The results emphasize the important effects of centrifugal force on the main motion in such a flow. In swirling flow, turbulence intensities are more pronounced compared to normal axial flow. Where the centrifugal force is important, near the inlet, axial and radial mean velocities are very disturbed. Thus, this force manages the flow motion and is responsible for a recirculating zone near the inner cylinder and for an anisotropic behaviour of the flow turbulence, where the strength of the swirl motion is higher.

Due to the decay of the circumferential velocity along the flow path, the swirl motion decreases to tend towards an axial flow with vanishing radial and tangential velocities, and a decay of turbulence intensities towards those observed in an axial flow is also seen. Nevertheless, in our experimental device, the swirl motion remains sensitive all along the length of the annulus, showing the strong tendency of a tangential inlet to induce swirling decaying flow. The swirl motion decay is characterized by an exponential evolution of the swirl number, S_n , with the axial distance. The dimensionless turbulent energy also follows an exponential decay, showing the great influence of the swirl intensity on hydrodynamic characteristics all along the length of the annulus axis. Finally, the non-axisymmetric behaviour of the flow is noted, making swirl motion difficult to fully investigate. However, as seen in this study, PIV appears well adapted to these investigations because accurate results can be obtained using a rather simple test procedure.

References

- Algifri AH; Bhardwaj RK; Rao YVN (1988) Eddy viscosity in decaying swirl flow in a pipe. *Appl Sci Research* 45: 287–302
- Aouabed H; Legentilhomme P; Nouar C; Legrand J (1994) Experimental comparison of electrochemical and dot-paint methods for the study of swirling flow. *J Appl Electrochem* 24: 619–625
- Aouabed H; Legentilhomme P; Legrand J (1995) Wall visualization of swirling decaying flow using a dot-paint method. *Exp Fluids* 19: 43–50
- Benisek M; Protik Z; Nedeljkovic M (1984) Investigation on the incompressible turbulent swirling flow characteristics change along straight circular pipes. *ZAMM. Angew Math Mech* 66: 195–197
- Brücker Ch (1996a) A new method for determination of the out-of-plane component in three-dimensional PIV using a color-coded light-sheet and spatial correlation: simulation and feasibility study for three-dimensional scanning PIV. *Int Mech Eng* 189–199
- Brücker Ch (1996b) 3D PIV via correlation in a color-coded light-sheet. *Exp Fluids* 21: 312–314
- Burfoot D; Rice P (1984) Heat transfer and pressure drop characteristics of alternative rotation swirl flow inducers in a circular duct. *Chem Eng Res Des* 62: 128–132
- Cenedese A; Doglia G; Romano GP; De Michele G; Tanzini G (1994) LDA and PIV velocity measurements in free jets. *Exp Therm Fluid Sci* 9: 125–134
- Cheng CY; Alkinson JF; Bursik M (1997) Direct measurement of turbulence structures in mixing jar using PIV. *J Environ Eng* 115–125
- Clayton BR; Morsi YSM (1984) Determination of principal characteristics of turbulent swirling flow along annuli. Part 1: Measurement of time mean parameters. *Int J Heat Fluid Flow* 5: 195–203
- Clayton BR; Morsi YSM (1985) Determination of principal characteristics of turbulent swirling flow along annuli. Part 2: Measurement of turbulence components. *Int J Heat Fluid Flow* 6: 31–41
- Escudier MP; Borstein J; Zehnder N (1980) Observations and LDA measurements of confined turbulent vortex flow. *J Fluid Mech* 98: 49–63
- Faler JH; Leibovitch S (1977) Disrupted states of vortex flow and vortex breakdown. *Phys Fluids* 20: 1385–1400
- Farias Neto SR (1997) Simulation numérique des écoulements annulaires non-établis de type axial et tourbillonnaire – Cas du transfert de matière. PhD thesis, University of Nantes (France)
- Farias Neto SR; Legentilhomme P; Legrand J (1998) Finite-element simulation of laminar swirling decaying flow induced by means of a tangential inlet in an annulus. *Comp Meth Appl Mech Eng* 165: 189–213
- Gupta A; Lilley DG; Syred N (1984) Swirl flow. Energy and engineering sciences series. Fun bridge, welh, UK: Abacus Press
- Hay N; West PD (1975) Heat transfer in free swirling flow in a pipe. *J Heat Transfer* 97: 411–416
- Hinze JO (1959) Turbulence. New York: McGraw-Hill Book Co
- Host-Madsen A; McCluskey DR (1994) On the accuracy and reliability of PIV measurements. 7th Int Symp on the Application of Laser Techniques to Fluid Mechanics 11–14 July 1994, Lisbon (Portugal)

- Host-Madsen A; Nielsen AH** (1998) Accuracy of PIV measurements in turbulent flows. 7th Eur Symp on Particle Characterization, 10–12 March 1998, Nürnberg (Germany)
- Ito S; Ogawa K; Kuroda C** (1980) Turbulent swirling flow in a circular pipe. *J Chem Eng Jap* 13: 6–10
- Khoo BC; Chew TC; Heng PS; Kong HK** (1992) Turbulence characterisation of a confined jet using PIV. *Exp Fluids* 13: 350–356
- Khoo BC; Yeo KS; Lim DF** (1997) The axisymmetric boundary layer beneath a Rankine-like vortex. *Exp Fluids* 22: 300–311
- Kito O; Kato T** (1985) Near wall velocity distribution of turbulent swirling flow in circular pipe. *Bull JSME* 27: 53–56
- Kölher U; Weichert R** (1998) Three-dimensional particle image velocimetry in turbulent flows. 7th Eur Symp on Particle Characterisation, pp. 255–263. Nürnberg (Germany)
- Korjack TA** (1985) Mass transfer of decaying products in swirling laminar pipe flow. *Powder Technol* 45: 57–62
- Kuroda C; Ogawa K; Inoue I** (1981) An approximate equation of axial velocity distribution in turbulent swirling pipe flow. *J Chem Eng Jap* 14: 158–160
- Legentilhomme P; Legrand J** (1991) The effects of inlet conditions on mass transfer in annular swirling decaying flow. *Int J Heat Mass Transfer* 34: 1281–1291
- Legrand J; Aouabed H; Legentilhomme P; Lefèbvre G; Huet F** (1997) Use of electrochemical sensors for the determination of wall turbulence characteristics in annular swirling decaying flows. *Exp Therm Fluid Sci* 15: 125–136
- Mungal MG; Lourenco LM; Krothapalli A** (1995) Instantaneous velocity measurements in laminar and turbulent premixed flames using on-line PIV. *Combust Sci Tech* 106: 239–265
- Nejad AS; Vanka SP; Favaloro SC; Samimy M; Langenfeld C** (1988) Application of laser velocimetry for characterisation of confined swirling flow. Symposium on the Gas Turbine and Aeroengine Congress and Exposition, 5–9 June 1988, Amsterdam (Netherlands) – Trans ASME 1–15
- Raffel M; Gharib M; Ronneberger O; Kompenhans J** (1995) Feasibility study of three-dimensional PIV by correlating images of particles within parallel light sheet planes. *Exp Fluids* 19: 69–77
- Saadeh M; Strauss K; Schneider T** (1997) A combined PIV/LIF-system for the measurements of heterogeneous drag reduction effects in a pipe-flow. *Exp Fluids* 22: 292–299
- Sethumadhavan R; Raja Rao M** (1983) Turbulent flow heat transfer and fluid friction in helical-wire-coil inserted tubes. *Int J Heat Mass Transfer* 26: 1833–1845
- Shi RX; Chehroudi B** (1994) Velocity characteristics of a confined highly turbulent swirling flow near a swirl plate. *J Fluids Eng* 116: 685–693
- Simmers DA; Coney JER** (1979) A Reynolds analogy for the heat transfer characteristics of combined Taylor vortex and axial flow. *Int J Heat Mass Transfer* 22: 679–689
- Yukawa H; Hashimoto M** (1982) Pressure drop in swirl flow through an annulus. *J Chin Ins Chem Eng* 13: 161–167